Very near-bottom tidal straining in a sea strait

Hans van Haren[1]

Received 2 June 2010; revised 9 July 2010; accepted 16 July 2010; published 26 August 2010.

[1] Large vertical temperature differences up to 3°C m^{-1} are observed very near (<0.5 m from) the 2-m sand-waves bottom in a 20–25 m deep sea strait dominated by tidal flows >1 m s^{-1}. The upper sensor at 0.42 m above the bottom (mab) follows typical temperature variations higher up in the water column, being −90° out-of-phase with the main along-channel current. In contrast, the lower sensor at 0.08 mab is approximately +30–50° more in-phase with the free-stream current. The data confirm the mechanism of "tidal straining", but much closer to the bottom than previously observed and in a 3-D version with cross-flow influences. In this mechanism, turbulent shear flow and horizontal density gradients create stable stratification during ebb and unstable conditions during flood. Here, stratification provides a slippery boundary flow-condition and periodic support of short-scale internal waves with periods down to 50 s. **Citation:** van Haren, H. (2010), Very near-bottom tidal straining in a sea strait, *Geophys. Res. Lett.*, *37*, L16603, doi:10.1029/2010GL044186.

1. Introduction

[2] In estuaries and sea straits that connect basins with waters of different density, oscillatory, mostly tidal, flows can generate periodically varying stratification: "tidal straining" [*Simpson et al.*, 1990]. As currents are subject to bottom friction they show vertical current variation ("shear") following turbulent mixing from the bottom upward. Due to this shear, initial horizontal density gradients, which are commonly positive towards the open "outer" sea, will create (more) stable vertical density stratification during ebb. This is because less-dense inland-sea water is moved over denser outer sea water. It also can cause near-homogeneous or convectively unstable situations during part of flood, when denser waters are displaced over less dense waters following erosion of stratification. The net result is periodic varying vertical turbulent exchange [e.g., *Rippeth et al.*, 2001; *Fisher et al.*, 2002; *Thorpe et al.*, 2008], which is commonly hampered by stratification. It also creates a net landward sediment transport [*Jay and Musiak*, 1994; *Scully and Friedrichs*, 2007; *Burchard et al.*, 2008].

[3] Tidal straining has been demonstrated from observations (references above [*Simpson et al.*, 2005; *Framiñan et al.*, 2008]) and from detailed modeling [e.g., *Burchard and Baumert*, 1998; *Li et al.*, 2008]. These all show mid-water or near-surface stratification and associated diminution in mixing above the frictional bottom boundary layer (bbl). *Simpson et al.* [1990] formulated a criterion for the minimum horizontal density gradient in the direction of tidal flow for which such strain-induced periodic stratification can be expected:

$$1/\rho\ \partial\rho/\partial x \approx 2.2 \times 10^{-5}(U/H)^2, \quad (1)$$

where ρ denotes the density, U the free-stream tidal current amplitude and H water depth.

[4] As will be shown here using near-bottom temperature measurements from a sea strait, tidal periodic stratification can also occur in the lower 1-m above the bottom. Contrary to stratification which is at the far edge of the bbl, this is the lowest part of bbl, where shear is expected to be largest. This lower 1-m is commonly modeled by a boundary condition of certain slip for overlying turbulent exchange in rotational Ekman dynamics. The spring-time observations are from a sea strait with modest sand-dunes, affecting the near-bottom flow.

2. Data and Handling

[5] A single 3x1 m almost flat, rectangular bottom-frame was moored in the Marsdiep at 52° 59.025′ N, 04° 46.876′ E, mean H = 23 m, between 28 and 31 May 2001. The Marsdiep is the 4.5 km wide, slightly curved sea-strait between the island of Texel to the north and the mainland to the south (Figure 1). It exchanges waters from the outer sandy North Sea to its West and the inland tidal-flat, muddy Wadden Sea to its East. Besides several other sensors (not discussed here) sticking vertically upward, the frame held an upward-looking 300 kHz broadband RDI-ADCP with its acoustic and temperature (T) sensors at 0.42 m above the bottom (mab) and a SeaBird SBE-26 pressure (p) recorder, with its p,T-sensors at 0.08 mab. The ADCP stored single ping-data every 1.85 s, sampling 44 vertical 0.5-m bins. First bin is 4.0 mab. The p-recorder sampled at 4 Hz, storing 2000 data before 100 s rest, every 600 s.

[6] Tilt sensors showed that the frame was on a 4.7° slope. Heading and tilt varied less than 0.1° due to currents, which implies that the instruments were well-fixed in position. The mean slope suggests the frame was on a steep side of an asymmetric sand wave, which on average has amplitude h = 2 m and wavelength L = 150 m, or 1.5° angle to the horizontal [*Buijsman and Ridderinkhof*, 2008]. Semidiurnal tidal current speeds exceed 1 m s^{-1} (see below), resulting in coarse sandy bottom sediment with grain sizes >400 μm [*Postma*, 1958]. In the water column, suspended matter consists of finer materials, classified as sand [*Postma*, 1954] or as silt, mean sizes of 25 μm, [*Merckelbach*, 2006]. Suspended matter loads at all depths are ~0.1 kg m^{-3}, except perhaps <1 mab [*van Haren*, 2009b]. Weather conditions were favorable, with some WSW5 winds during the first 2 days, and virtually no wind later in the week.

[7] Current data are rotated by 19° to the North of East, the local direction of the average principal tidal ellipse axis. T-data from the p-recorder (T_p) were well-calibrated and more precise than T_{ADCP}: ±0.01°C and ±0.4°C accuracy,

[1]Royal Netherlands Institute for Sea Research, Den Burg, Netherlands.

0094-8276/10/2010GL044186

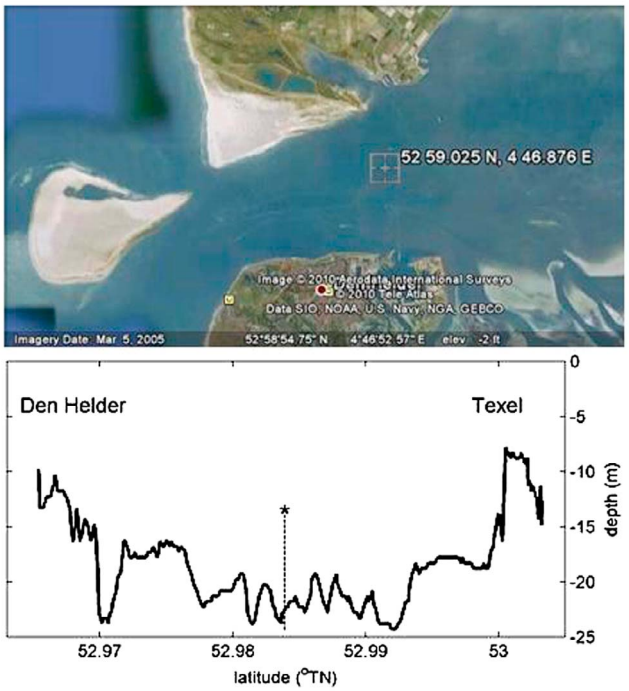

Figure 1. Marsdiep (*) with mooring location (Google Earth) and transect with bottom topography (shipborne ADCP-data).

respectively. As only 600 s average T_p-data are recorded, raw T_{ADCP} are averaged to have the same sampling interval for comparison.

[8] Between days 148.36 and 148.75 shipborne Seabird SBE-911 CTD-observations were made, one vertical profile every 1200 s. The accuracy of T_{CTD} is ±0.002°C. Observations were made during 13 hours, to cover one tidal period, but the ship had to change position twice during maximum flood, because the anchor could not be held and because "too much suspended material whirled up". Here, only data from one position are shown (52° 59.187′ N, 04° 46.687′ E), about 450 m NW of the mooring. The CTD-data are processed in 0.25 m vertical bins, starting at 1.5–2.5 m from the surface and extending to 1–1.5 mab.

[9] Comparison between near-bottom moored T and nearest T_{CTD} resulted in some corrections, for relatively inaccurate T_{ADCP}. However, a direct comparison between T-data is not possible. Firstly, the CTD did not range as close to the bottom as where the moored sensors were. Secondly, ship and mooring were not at the same horizontal position. This can be partially corrected using ADCP's current information and shifting time of the CTD-data, assuming no variations in water column structure over the period of advection across 450±100 m. No correction can be made for difference in local water depths, about 2 m, and different bottom (sand wave) structures. Anchor-sway (flood-ebb) implies a horizontal displacement of the size of L. Local tidal range is about 1.5 m, which is smaller than typical h.

3. Observations

[10] End of May, water in the Wadden Sea is already warmer than in the North Sea. This implies that salt (S) and temperature act both positively to buoyancy, thereby creating a relatively large gradient between the warmer and fresher inland waters and the cooler, saltier outer sea waters (Figure 2). T-S relationship (Figure 2a) always has the same sign of slope but its magnitude varies strongly between Wadden Sea water, with mostly S contributing to density variations, and North Sea water, with T and S contributing about equally to density variations. Estimating from CTD-observations and the tidal current excursion length of 18 km, the average along-channel density gradient amounts $\Delta\rho/\Delta x = 1.5\pm0.4 \times 10^{-4}$ kg m^{-4}. This is in the same range as in Liverpool Bay [*Simpson et al.*, 1990] and about twice the minimum value (1) for typical U. So, one can expect tidal straining to be effective.

[11] During flood (dashed profiles in Figure 2b) stratification in the interior can become unstable over the entire range measured, but only for a few (3) profiles. Then, on average typical stratification is weak, but measurable, O(0.01) kg m^{-3} over the vertical range (Figures 2b and 2c), resulting in buoyancy periods T_N = 1000–3000 s. Already before high water, near–surface stratification increases to about $d\rho/dz \approx 0.1$ kg m^{-4} providing buoyancy periods $T_N \approx 200$ s. This near-surface stratification is presumably caused by estuarine (cross-) circulation. During ebb typically $T_N \approx 100$–300 s is observed, in the upper half of the water column, with slowly decreasing stratification in the lower half.

[12] In the near-bottom layer, currents are expected to provide large shear between the fast flow in the interior and the bottom. The moored T-sensors show tidally varying temperature and T-stratification between 0.08 and 0.42 mab (Figures 3a and 3b). Difference ΔT = 1–1.5°C, but also occasionally shows unstable periods, as far as can be judged from the differently calibrated sensors. Using conservatively the North Sea T-S relationship for converting ΔT to buoyancy periods, one arrives at $T_N \approx 50$ s (period of strongest stratification; second half ebb - low water) and $T_N \approx 300$ s - ∞ (weak stratification-instability; second half flood). Wadden Sea T-S results in T_N-values smaller by a factor of 2.2. The former stratification is stronger than observed near the surface; the latter is typical for the interior lower half during ebb and beginning of flood. Note the timing differences of near-surface and near-bottom stratification. The latter is about −90° out-of-phase with the main tidal current, which is precisely expected for [near-surface] tidal straining driven by along-channel current.

[13] The two near-bottom T-records show a completely different variation with time, except for the common slow T-increase over the entire period of measurements. The upper sensor shows mostly, but not always, warmer values, with a tidal periodicity that is about −90° out-of-phase with the horizontal along-channel current. During upcoming flood T rapidly drops by half a degree and slowly decreases or remains stable for the first hour of peak flood. During or just after that hour, the lower, generally cooler sensor shows a relatively sudden increase of about 0.2°C, before decreasing with near-equal values as the upper sensor. The sudden increase at the lower sensor during flood follows a period of near-constant, or weakly decreasing values during ebb, with weakly minimum values found about 2 hours after peak ebb. As a result, the lower sensor record follows the horizontal along-channel current with a phase lag of 30–50°, but its variation with time is more saw–tooth than sinusoidal in shape and overall its amplitude is much smaller than that of the upper sensor.

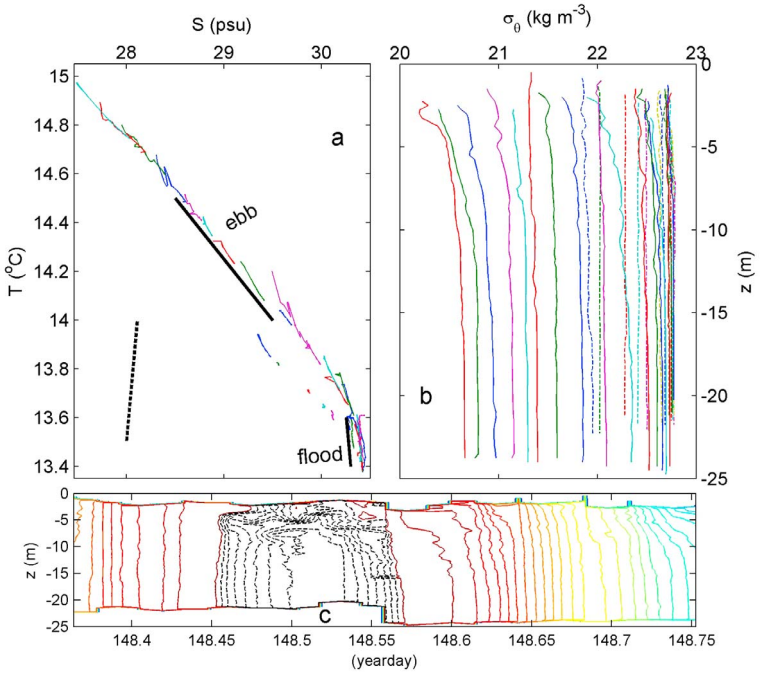

Figure 2. CTD-data obtained roughly between 350 (flood) and 550 m (ebb) NW of the mooring, every 1200 s between days 148.3639 (flood) and 148.75 (ebb). (a) Temperature-salinity diagram for profiles in Figure 2b using the same colours. Black lines indicate tight T-S relationships: lower right (North Sea water) $-\partial T/\partial S = -4.5$, upper (Wadden Sea water) $-\partial T/\partial S = -1/3$; the canonical $-(\partial T/\partial S)\rho = 4.5$ is dashed (thus indicating a line of approximate constant density). (b) Potential density referenced to the surface. Profiles are not off-set deliberately; dashed profiles indicate flood, solid profiles ebb. (c) Contours of constant density, every 0.1 kg m^{-3} (color) and every 0.01 kg m^{-3} (black-dashed). High-water is at day 148.52 (the 'c').

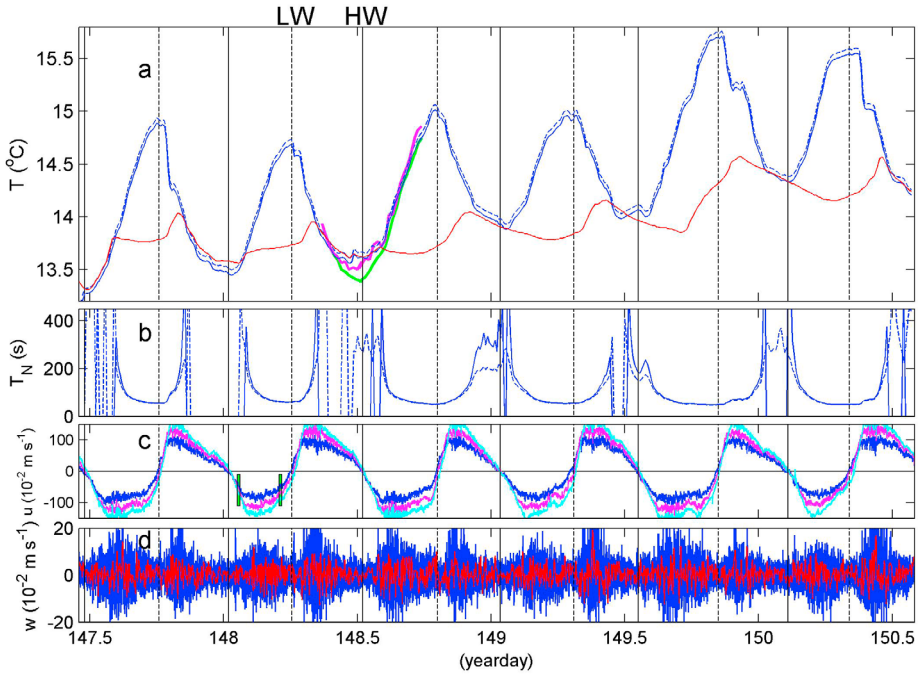

Figure 3. Time series of moored observations. (a) T_{ADCP} at 0.42 mab (blue-dashed; after correction (see text): solid) and T_P at 0.08 mab (red). Near-surface T_{CTD} (purple) and near-bottom T_{CTD} (green). (b) Buoyancy frequency computed between the two solid T-graphs of a. (solid) and between dashed and lower solid graphs (dashed), using a conservative $\delta\rho$-δT relationship for North Sea waters (effective contraction coefficient of 4×10^{-4} °C^{-1}). (c) Low-pass (600 s cut-off) filtered along-channel current component (19° North of East) at 4.5 (blue), 11 (purple) and 17.5 mab (light-blue). (d) Band-pass filtered vertical current measured at 4.5 mab; low-pass cut-off at 3 hours, high-pass at 16 s (blue) and 400 s (red).

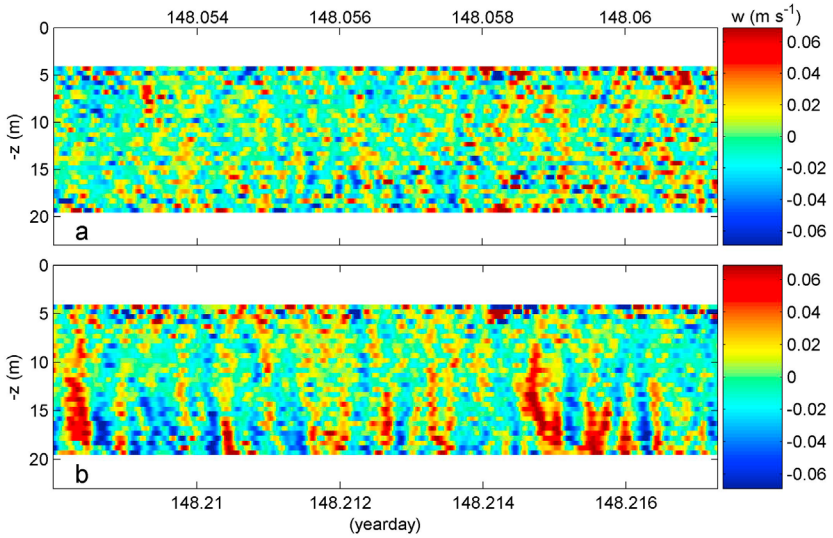

Figure 4. Depth-time (800 s) series of [3-h, 16-s] band-pass filtered w when $|U| \approx 0.6$ m s^{-1}, half-maximum value. (a) Start of ebb, near-homogeneous. (b) End of ebb, strongly stratified.

[14] During about 5 hours in any tidal period, more or less evenly distributed around high water, the two sensors provide nearly the same values, with on average slightly higher values for the upper sensor. During these periods, this upper sensor shows a deviation from a sinusoidal variation, as the T-trough is flattened and more ruggedly varying with time. Occasionally during this part of the tidal phase, T-instabilities are observed. In contrast, the near-bottom (1–1.5 mab) T_{CTD} shows a more sinusoidal shape, but the near-surface one less so (Figure 3a). After "correcting" T_{CTD} for the mismatch in horizontal positioning, which generally works well except during high water, T_{ADCP} resembles more T_{CTD} than T_p. However, it still seems too high by about 0.05°C as during ebb its value lies between that of the upper and lower CTD-values. This correction-value corresponds to the average horizontal T-gradient between the ship and the mooring, by chance. Recalling the large uncertainty in T_{ADCP} it may represent bias, albeit somewhat speculative. Using it as corrective (Figure 3a solid curves) results in nearly equal T_{ADCP} and near-bottom T_{CTD} during most of ebb and nearly equal T_{ADCP} and near-surface T_{CTD} during part of flood. Unexplained are $T_{CTD} > T_{ADCP}$ during mid-flood (beginning of CTD record), when also $T_p > T_{ADCP}$. Also unexplained remains the high-water trough in near-bottom T_{CTD}, which may have to do with different positioning of the ship compared to the mooring in relation to sand waves.

[15] The observed currents between 4.5 and 17.5 mab show a near-linear decrease with depth, but at 4.5 mab maximum speeds are still 1 m s^{-1}. Phase variation is only some 2° (visible in Figure 3c, low water-flood), with the current-ellipse veering anticlockwise, as expected for oscillating flows on a rotating Earth in the northern hemisphere [*Prandle*, 1982; *Maas and van Haren*, 1987]. Thus, rotational effects are not negligible in such a narrow strait, with near-rectilinear tidal motions. In the ADCP-range shear amounts up to 0.03 s^{-1}, which can be supported by stratification of $T_N \geq 400$ s, invoking gradient Richardson number Ri = 0.25, High-frequency motions, noise, turbulence and/or internal waves are largest near peak mean tidal flows. This is best visible in near-bottom (still 4.5 mab) vertical currents w (Figure 3d), which show most energetic fluctuations during moments of transition between stratified and unstable water column, but always when near-bottom stratification has finite values and flows are maximal (Figure 3c). Part of these w are suppressed during ebb of strongest near-bottom stratification, indicative of less turbulence activity. If the band-pass filter shifts to slightly lower frequencies (red graph in Figure 3d) we see that fluctuating w maintain their amplitude throughout the stratified ebb-phase and show smallest values during the near-homogeneous "unstable" flood-phase (Figure 4). This suggests high-frequency internal wave activity besides turbulent, possible sand-wave-induced, w. Observed wave periods can be as short as 50 s (Figure 4b), commensurate near-bottom T_N. Largest |w| are observed closest to the bottom suggesting the waveguide below 4.5 mab [*van Haren*, 2009a]. Vertical extent of w is about half-way the water column and commonly much larger than interfacial displacement. As for their generation, tidal flow interacting with sand waves is plausible.

4. Discussion

[16] A sea strait like the Marsdiep is a complex region where processes like estuarine cross-flow circulation (driven by horizontal density gradients and curvature) occur next to tidal straining (driven by bottom frictional tidal flow in the presence of horizontal density gradients). The strong tidal current prevents permanent settling of fine silt at the bottom, whilst transporting it throughout the water column. It also causes bed-load transport and sand waves formation and displacement. In contrast with previous studies, tidal straining is more clearly observed very close to the bottom. Question is why.

[17] The bottom structure (its degree of flatness) and texture (grain-size and -packing) together with turbulence due to frictional shear set a boundary condition for interior flow with varying degree of slip. In a linear flow this creates a log-profile of varying exponent in approximately the lower 1 mab [*Gust and Weatherly*, 1985]. In areas with sand waves such profiles become more heavily distorted, but still have the

same characteristics in which just decay rates vary [*van Gastel*, 1987]. In an oscillatory flow such profile will show reverse flow near the bottom during part of the cycle [*Lamb*, 1932]. In a rotating frame of reference it will show cross-flow and -shear due to Ekman dynamics, with near-bottom flows preceding those higher-up. This is a result of turbulent exchange being different for flows that are counter- and co-rotating with Earth rotation [*Prandle*, 1982]. Thus tidally strained stratification will in turn modify the flow, with larger phase variation the closer it gets to the bottom [*van Haren and Maas*, 1987]. This stratification may partially be intensified by suspended sediments with typical loads of 0.1 kg m^{-3}, although these are observed at all depths. Thus, near-bottom frictional effects of oscillatory flows in a rotating frame modified by stratification and sand-waves cause very strong current veering which enhances the stratification during part of the tidal phase.

[18] As expected for tidal straining, the present near-bottom observations show very little stratification during the second part of flood due to erosion. During ebb one expects strong stratification, which is indeed also observed by the moored near-bottom sensors. However, the cooling at the lowest sensor during this period points at an additional mechanism. This cooling is not attributable to sensor burying in the sand or mud, as this would rather increase, certainly not decrease, T during ebb-flow. The large phase differences between the two sensors, becoming about 140°, point at a near-bottom frictional current advecting a South-North temperature gradient. The latter is observed in the CTD-mooring data comparison, albeit at different depths. This would evidence Ekman spiral rotation very close to the bottom, but the frictional aspect is hard to distinguish from the transverse density gradient forcing. This requires further investigation.

[19] The result is a very slippery boundary layer during stratified periods, which may hamper vertical exchange, but in turn can generate high-frequency internal waves locally.

[20] **Acknowledgments.** I enjoyed the assistance of the crew of the R.V. Navicula. I thank Theo Hillebrand for preparing and deploying the instruments, Frans Eijgenraam for topographical data and Eric Epping, John Simpson, Hans Burchard, Lars Umlauf and anonymous referees for advice.

References

Buijsman, M. C., and H. Ridderinkhof (2008), Long-term evolution of sand waves in the Marsdiep inlet. I: High-resolution observations, *Cont. Shelf Res.*, *28*, 1190–1201, doi:10.1016/j.csr.2007.10.011.

Burchard, H., and H. Baumert (1998), The formation of estuarine turbidity maxima due to density effects in the salt wedge. A hydrodynamic process study, *J. Phys. Oceanogr.*, *28*, 309–321, doi:10.1175/1520-0485(1998)028<0309:TFOETM>2.0.CO;2.

Burchard, H., G. Flöser, J. V. Staneva, T. H. Badewien, and R. Riethmüller (2008), Impact of density gradients on net sediment transport into the Wadden Sea, *J. Phys. Oceanogr.*, *38*, 566–587, doi:10.1175/2007JPO3796.1.

Fisher, N. R., J. H. Simpson, and M. J. Howarth (2002), Turbulent dissipation in the Rhine ROFI forced by tidal flow and wind stress, *J. Sea Res.*, *48*, 249–258, doi:10.1016/S1385-1101(02)00194-6.

Framiñan, M. B., A. Valle-Levinson, H. H. Sepúlveda, and O. B. Brown (2008), Tidal variations of flow convergence, shear, and stratification at the Rio de la Plata estuary turbidity front, *J. Geophys. Res.*, *113*, C08035, doi:10.1029/2006JC004038.

Gust, G., and G. L. Weatherly (1985), Velocities, turbulence, and skin friction in a deep-sea logarithmic layer, *J. Geophys. Res.*, *90*, 4779–4792, doi:10.1029/JC090iC03p04779.

Jay, D. A., and J. D. Musiak (1994), Particle trapping in estuarine tidal flows, *J. Geophys. Res.*, *99*, 20,445–20,461, doi:10.1029/94JC00971.

Lamb, S. H. (1932), *Hydrodynamics*, 738 pp., Dover, New York.

Li, M., J. Trowbridge, and R. Geyer (2008), Asymmetric tidal mixing due to the horizontal density gradient, *J. Phys. Oceanogr.*, *38*, 418–434, doi:10.1175/2007JPO3372.1.

Maas, L. R. M., and J. J. M. van Haren (1987), Observations on the vertical structure of tidal and inertial currents in the central North Sea, *J. Mar. Res.*, *45*, 293–318, doi:10.1357/002224087788401106.

Merckelbach, L. M. (2006), A model for high-frequency acoustic Doppler current profiler backscatter from suspended sediment in strong currents, *Cont. Shelf Res.*, *26*, 1316–1335, doi:10.1016/j.csr.2006.04.009.

Postma, H. (1954), Hydrography of the Dutch Wadden Sea, *Arch. Neerl. Zool.*, *10*, 405–511, doi:10.1163/036551654X00087.

Postma, H. (1958), Size frequency distribution of sands in the Dutch Wadden Sea, *Arch. Neerl. Zool.*, *12*, 319–350, doi:10.1163/036551658X00029.

Prandle, D. (1982), The vertical structure of tidal currents, *Geophys. Astrophys. Fluid Dyn.*, *22*, 29–49, doi:10.1080/03091928208221735.

Rippeth, T. P., N. R. Fisher, and J. H. Simpson (2001), The cycle of turbulent dissipation in the presence of tidal straining, *J. Phys. Oceanogr.*, *31*, 2458–2471, doi:10.1175/1520-0485(2001)031<2458:TCOTDI>2.0.CO;2.

Scully, M. E., and C. T. Friedrichs (2007), Sediment pumping by tidal asymmetry in a partially mixed estuary, *J. Geophys. Res.*, *112*, C07028, doi:10.1029/2006JC003784.

Simpson, J. H., J. Brown, J. Matthews, and G. Allen (1990), Tidal straining, density currents, and stirring in the control of estuarine stratification, *Estuaries*, *13*, 125–132, doi:10.2307/1351581.

Simpson, J. H., E. Williams, L. H. Brasseur, and J. M. Brubaker (2005), The impact of tidal straining on the cycle of turbulence in a partially stratified estuary, *Cont. Shelf Res.*, *25*, 51–64, doi:10.1016/j.csr.2004.08.003.

Thorpe, S. A., J. A. M. Green, J. H. Simpson, T. R. Osborn, and W. A. M. Nimmo Smith (2008), Boils and turbulence in a weakly stratified shallow tidal sea, *J. Phys. Oceanogr.*, *38*, 1711–1730, doi:10.1175/2008JPO3931.1.

van Gastel, K. (1987), Velocity profiles of tidal currents over sand waves, *Neth. J. Sea Res.*, *21*, 159–170.

van Haren, H. (2009a), High-frequency vertical current observations in stratified seas and ocean, *Cont. Shelf Res.*, *29*, 1251–1263, doi:10.1016/j.csr.2009.02.002.

van Haren, H. (2009b), Ship-induced effects on bottom-mounted acoustic current meters in shallow seas, *Cont. Shelf Res.*, *29*, 1809–1814, doi:10.1016/j.csr.2009.06.002.

van Haren, J. J. M., and L. R. M. Maas (1987), Temperature and current fluctuations due to tidal advection of a front, *Neth. J. Sea Res.*, *21*, 79–94, doi:10.1016/0077-7579(87)90024-X.

H. van Haren, Royal Netherlands Institute for Sea Research, PO Box 59, NL-1790 AB Den Burg, Netherlands. (hans.van.haren@nioz.nl)